INTERNATIONAL JOURNAL FOR NUMERICAL METHODS IN FLUIDS
Int. J. Numer. Meth. Fluids 2003; **41**:633–652 (DOI: 10.1002/fld.460)

Bulk viscosity damping for accelerating convergence of low Mach number Euler solvers

Karim Mazaheri[1,*,†] and Philip L. Roe[2]

[1]*Sharif University of Technology, Tehran 11635-8639, Iran*
[2]*The University of Michigan, Ann Arbor, Michigan 48109, U.S.A.*

SUMMARY

In solution of the Euler equations in the steady state external flows, error or residual waves are blamed for decelerating the convergence. These waves may be damped by adding a bulk viscosity term to the momentum equations. We analyse effects of this term on the linearized differential equations, and study its explicit and implicit implementation in one and two space dimensions. Optimum values of the bulk viscosity damping (BVD) are discussed. After generalization to two space dimensions, its performance both alone and in combination with a soft wall boundary condition and residual smoothing in central differencing codes is reviewed. It is shown that BVD is complementary to them, and acts independently of them. Finally, application of BVD in solution of low Mach number flows is considered, to show how it can strongly stabilize and accelerate these low Mach number computations. Copyright © 2003 John Wiley & Sons, Ltd.

KEY WORDS: convergence acceleration; Euler solvers; bulk viscosity damping

1. INTRODUCTION

In two space dimensions, the time-dependent Euler equations are

$$\frac{\partial}{\partial t}\begin{pmatrix}\rho\\ \rho u\\ \rho v\\ \rho E\end{pmatrix}+\frac{\partial}{\partial x}\begin{pmatrix}\rho u\\ \rho u^2+p\\ \rho uv\\ \rho uH\end{pmatrix}+\frac{\partial}{\partial y}\begin{pmatrix}\rho v\\ \rho uv\\ \rho v^2+p\\ \rho vH\end{pmatrix}=\mathcal{O} \tag{1}$$

Here, ρ is density, u and v are velocity components, p is pressure, and E and H are total internal energy and total enthalpy, respectively. For $\mathbf{u}$ the vector of primitive variables,

* Correspondence to: K. Mazaheri, Sharif University of Technology, Tehran, 11365-8639, Iran.
† E-mail: mazaheri@sharif.edu

Received 3 March 2002
Revised 1 November 2002

(ρ, u, v, p), simple wave solutions could be written in the form

$$\mathbf{u} = \mathbf{u}(\mathbf{x}\cos\theta + \mathbf{y}\sin\theta - \lambda t)$$

which indeed shows solutions which are constant on straight lines in 'xy' plane, moving with characteristic speed λ in the direction of its unit normal $\mathbf{n} = (\cos\theta, \sin\theta)$. The characteristic surfaces are moving with corresponding speeds.

It is interesting to note that in numerical solution of the Euler equations for the steady state problems (and many other fluid dynamics equations), the errors and the residuals of the conserved variables are convected, dispersed and dissipated like a scalar quantity. Therefore, it is natural to study the behaviour of these waves to develop any technique which involves them, particularly in convergence acceleration methods. To do so, techniques were developed to allow experimental study of the residual waves [1]. Video films were made which show how the solution evolves. A simple first-order upwind scheme using local time-stepping on a rather coarse structured grid was used to find the solution of the Euler equations around a NACA0012 airfoil at $M = 0.63$ and $\alpha = 2°$. Contours of area-weighted residuals (Cell Area $\times$ $|\rho_t|$) were found to be a very simple way for visualization of evolution of error waves. The area weighting was used as a way of emphasizing the far field behaviour. The video revealed very clearly that the path to convergence follows a simple, well-defined, repetitive pattern that begins almost immediately. For the first cycles, there are minor variations, but after this each cycle repeats the previous one very faithfully. A perfect correlation is maintained between the timing of the residual waves, and the '*beating*' in a conventional residual history (as in *Figure* 9).

An additional observation, suggesting that acoustic behaviour is almost completely dominant, comes from correlating the pressure and density residuals. For any purely acoustic disturbance, one should find that

$$p_t = a^2 \rho_t \tag{2}$$

In fact, one finds that this equation holds to within 1% on average over the flow field.

All of these observations are convincing evidence that acoustic waves are responsible for an important part of the convergence process. After one basic cycle, i.e. the time required for the residual waves to traverse once the computational flow field (forward and backward, from airfoil to the outer boundary, and reverse) the amplitude of the residual waves can be expected to be reduced by a factor of something like

$$R = R_f R_o R_i \tag{3}$$

where R_f is the attenuation due to numerical dissipation (whether by accident or design) as the waves traverse the flow field twice, R_o is the attenuation when the waves reflect from the outer boundary, and R_i is the attenuation when the waves reflect from the inner solid boundary. It is believed that these facts should provoke a complete re-examination of boundary procedures and numerical schemes. In Reference [1] work is conducted which is aimed at preventing the regeneration of residuals by attenuating these continued reflections at the other end of their journey; that is, at the solid surface. In Reference [2] techniques are shown to decrease R_o.

An effective strategy to accelerate convergence of Euler solvers in solution of steady state problems, is to damp the residual waves while they are traversing the flow field. There are several ways to do this, like residual smoothing [3], classic multigrid [4] or newer ideas

as [5], which are nowadays the most popular convergence acceleration schemes. Preconditioning schemes as [6] help damping residual waves by speeding up the slow running waves. Here one systematic and very simple way is developed to do this. The idea generalizes one presented by Ramshaw and Mousseau [7] for accelerating the convergence of incompressible flow calculations. They added an *artificial bulk viscosity* term to a code based on the artificial compressibility method introduced in 1967 by Chorin [8]. Apparently nobody has tried to use this idea in genuinely compressible calculations. To do this, we have to take a slightly non-physical approach, so that the added terms vanish in the steady state. In this paper we construct an *artificial bulk viscosity*, which does vanish when required, and can be tuned to damp out the error waves, based on the fact that the acoustic waves are primarily responsible for the slow convergence. Physically, the most direct way to damp these components of the residual waves is by bulk viscosity damping (*BVD*). Thus it is natural to introduce an artificial bulk viscosity to remove these waves from the flow field.

In this paper we will first show why and how bulk viscosity affects our solution. Using one dimensional analysis, stability criteria are developed for the newly introduced parameter, and then BVD is applied in one-dimensional Euler equations, both explicitly and implicitly. Generalization to two space dimensions follows readily, and it is shown that this method is complementary to many other convergence accelerator schemes, including residual smoothing [9] and soft wall boundary conditions [1]. The remarkable effect of BVD in acceleration of Euler solvers in low subsonic regime is particularly studied at the end.

2. THEORY OF THE BULK VISCOSITY DAMPING (BVD)

The *Navier Stokes* momentum equation can be written as:

$$\frac{\partial}{\partial t}(\rho \mathbf{u}) + \mathrm{div}(\rho \mathbf{u} : \mathbf{u}) = \nabla \cdot \mathbf{T}$$

where the stress tensor $\mathbf{T}$ includes three terms:

$$\mathbf{T} = -p\delta_{ij} + \lambda\, \mathrm{div}(\mathbf{u})\delta_{ij} + 2\mu\varepsilon_{ij} \tag{4}$$

Here, $\mathbf{u}$ is the velocity vector, λ and μ are, respectively, the bulk viscosity and the shear viscosity coefficients, and body forces are neglected. ε is the strain rate tensor. The bulk viscosity is the part of the viscous stress which is proportional to the divergence of the velocity. For positive λ, bulk viscosity increases the internal energy proportional to $(\mathrm{div}(\mathbf{u}))^2$ and dissipates the acoustic waves.

For incompressible flow the velocity divergence vanishes in the steady state, and adding an artificial term proportional to it will leave the steady state unchanged. This was the approach taken in Reference [7]. For compressible flow, a similar effect can be achieved using the divergence of $\rho\mathbf{u}$, that is to say, $-\rho_t$. This also makes the dissipation of error waves proportional to square of their magnitudes.

For computation with the inviscid equations, we use

$$\mathbf{T} = -(p + a_o l \rho_t)\delta_{ij} \tag{5}$$

where a_o is the reference sound speed and l is an artificial bulk viscosity coefficient with the dimension of length. This constant needs to be determined by design criteria, or stability restrictions (found by analysis, or empirically).

To analyse the effect of the new term, *the linearized Euler equations* (i.e. *acoustic equations*) in one space dimension are considered first. After adding the new term we have:

$$\begin{aligned} \rho_t + \rho_o u_x &= 0 \\ u_t + \frac{1}{\rho_o} p_x + \frac{a_o l}{\rho_o} \rho_{xt} &= 0 \\ p_t + \rho_o a_o^2 u_x &= 0 \end{aligned} \tag{6}$$

Let us require simple wave solutions of the form:

$$\mathbf{u} = \mathscr{R}e(U) \exp \mathrm{i}(\omega t - \xi x)$$

for the vector of primitive variables $\mathbf{u}$, where ω is complex frequency, and ξ is the wave number. Here, $\mathscr{I}m(\xi) = 0$, in order to have bounded solutions for large x, but $\omega = \omega_r + \mathrm{i}\omega_i$. Substitution of this form of solution in the above equations, and requiring non-trivial solutions, yields the dispersion relation.

After some algebra one finds two different cases:

- $\omega_r = 0$, and

$$\frac{\omega_i l}{a_o} = (l\xi)^2 \left(\frac{1}{2} \pm \sqrt{\frac{1}{4} - \left(\frac{1}{l\xi} \right)^2} \right)$$

  which is only valid for $(l\xi)^2 \geqslant 4$.
- $\omega_i = \frac{1}{2} a_o l \xi^2$, and

$$\frac{\omega_r}{\xi a_o} = \pm \sqrt{1 - \left(\frac{l\xi}{2} \right)^2}$$

  for $(l\xi)^2 < 4$.

The variation of non-dimensionalized wave speeds $\omega_r/\xi a_0$ and damping $\mathrm{e}^{-\omega_i l/a_o}$ for different wave numbers are plotted in Figure 1. Figure 1(a) shows that high frequencies are heavily damped. Figure 1(b) shows that on the differential level the high frequencies are not allowed to propagate at all, which is in a sense an advantage, since then one will not be worried about their reflections from the boundaries, and their movements forward and backward in the flow field. At the same time, the advantage of convecting them out of the flow field is lost.

To see effects of the new term on the stability, we consider the following system of equations:

$$\begin{aligned} u_t + \frac{1}{\rho_o} p_x &= a_o l u_{xx} \\ p_t + \rho_o a_o^2 u_x &= 0 \end{aligned} \tag{7}$$

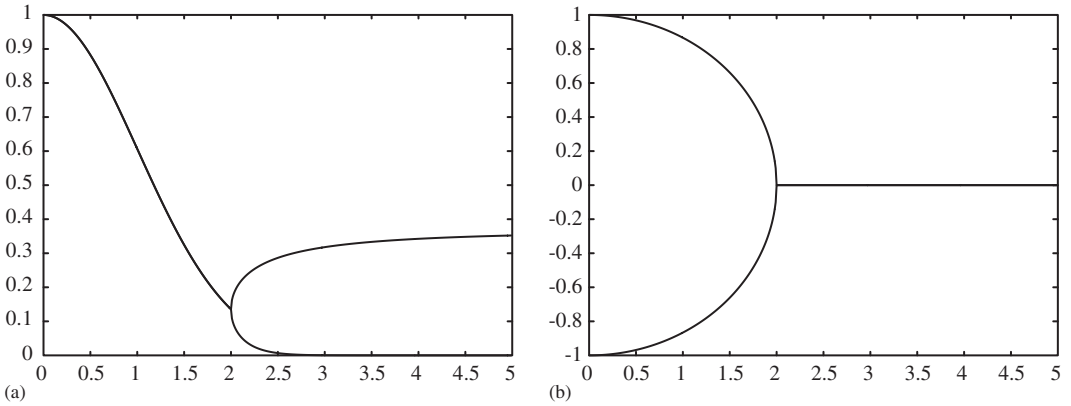

Figure 1. (a) Damping ($e^{-\omega_i l/a_o}$) and (b) wave speed ($\omega_r/\xi a_o$) for different wave numbers $l\xi$.

Analytically, these have the same dispersion relationship (apart from a non-propagating factor) as (6). One can write the equations in the characteristic form. Using central differencing for second order derivatives, and upwind differencing for the others, and assuming solutions of the form $\mathbf{u}_j^n = U_o \exp \mathrm{i}(n\Omega + j\beta)$ one finds the discrete amplification matrix. If v is *the Courant number*, to have bounded solutions we restrict eigen values of the amplification matrix and find

$$\frac{l}{\Delta x} \leqslant \left(\frac{1-v}{2v}\right) \tag{8}$$

Thus for a simple explicit discretization, the coefficient l cannot be large compared with the mesh size. This is natural, since we have added a parabolic term to the equations. In practice, as will be seen in the next sections, the stability margin on practical stencils is slightly wider than what this estimate suggests. If the pressure gradient term in the acoustic Equations (6) is neglected, one gets

$$u_t = l a_o u_{xx} \tag{9}$$

which is of parabolic nature. This shows that the added term acts like a singular perturbation of the original hyperbolic equations, and generates stiffness in the equations.

3. APPLICATION IN ONE SPACE DIMENSION

3.1. Explicit computations

After application of the above modifications to Equations (1), the resulting equations are

$$\begin{pmatrix} \rho \\ \rho u \\ \rho E \end{pmatrix}_t + \begin{pmatrix} \rho u \\ \rho u^2 + p \\ \rho u H \end{pmatrix}_x = \begin{pmatrix} 0 \\ -l a_o \rho_{xt} \\ 0 \end{pmatrix}$$

Indeed similar terms could also be added to the energy equation. However, the order analysis shows that this term will be proportional to l^2, so in explicit computations, where $l \approx \Delta x$ this term will be of higher order, and will not affect the solution.

The numerical method used here is an explicit upwind method (Extension to central differencing schemes follows in Section 5). The update procedure for the momentum equation will be slightly different:

$$(\rho u)_j^{n+1} = (\rho u)_j^n - \frac{\Delta t}{\Delta x}(F_{2,j+1/2}^{\star n} + F_{2,j-1/2}^{\star n}) - l a_o \frac{(\rho_t)_{j+1}^n - (\rho_t)_{j-1}^n}{2\Delta x}$$

where

$$(\rho_t)_j^n = -\frac{F_{1,j+1/2}^{\star n} + F_{1,j-1/2}^{\star n}}{\Delta x}$$

and $F_{2,j+1/2}^{\star n}$ is the second element of the flux vector, evaluated at the interface of cells j and $j+1$ at time step n (here computed using the Roe averages, but any good flux formula could be used). This seems to be the simplest way to create a discretization that is conservative, and for which the added terms vanish in the steady state. However, the stencil is effectively extended to five cells by the form of the BVD term. This appears to enlarge the stability margins found in the previous section. The boundary conditions for the extra term are applied using ghost cells, and ρ_t in the ghost cells is chosen to be zero.

To see the effect of the new term on the evolution of the solution in the flow field, computations are done in a pressure tube. Assume $0 < x < 1$ and $t > 0$. Solid walls are assumed at both ends. For the initial condition, the fluid is assumed to be still everywhere, with uniform density ρ_o, and with Gaussian distribution for pressure:

$$u = 0 \quad \rho = \rho_o \quad p = p_o(1 + \alpha e^{-\beta(x-0.5)^2})$$

where β is a constant of order 100. α is a constant equal to 0.1 or 1.0 which determines the strength of the initial pressure disturbance. Choosing $\alpha = 1.0$ will allow non-linear waves be generated in the flow field, which will collapse in a very strong shock wave. Using a global time-stepping procedure, Figure 2 shows the wave evolutions for $\alpha = 0.1$, which is weak enough to stay linear, with no bulk viscosity. The horizontal axis is the space dimension, $0 < x < 1$, and the vertical axis is time. The curves shown are pressure distributions at different times; the lower curve is the initial condition.

In Figure 2 the (almost perfect) reflection of the right and left-going waves at the solid wall can be observed. This figure shows that although a first-order dissipative method is used, the waves will bounce back and forth several times, before being dissipated in the flow field. Figure 3 shows how the smooth waves are dissipated fairly effectively in the first period of their movement, after addition of slight bulk viscosity with $l = \Delta x/2$. With this value of l, the regular explicit time step for the unmodified problem could be used.

To see how everything works at a non-linear level, an initial pressure distribution with high amplitude (i.e. $\alpha = 1$) is used. Figure 4 shows that in absence of bulk viscosity damping, strong shock waves are generated. Again, even in our first-order upwind code, shocks will move forward and backward for many cycles, before they are suitably damped.

Figure 5 shows that addition of small bulk viscosity ($l = \Delta x/2$) (small enough to keep the same time-steps stable) not only prohibits the shock from being generated, but also dissipates the wave as well before it accomplishes its first round trip. The amount of extra computation

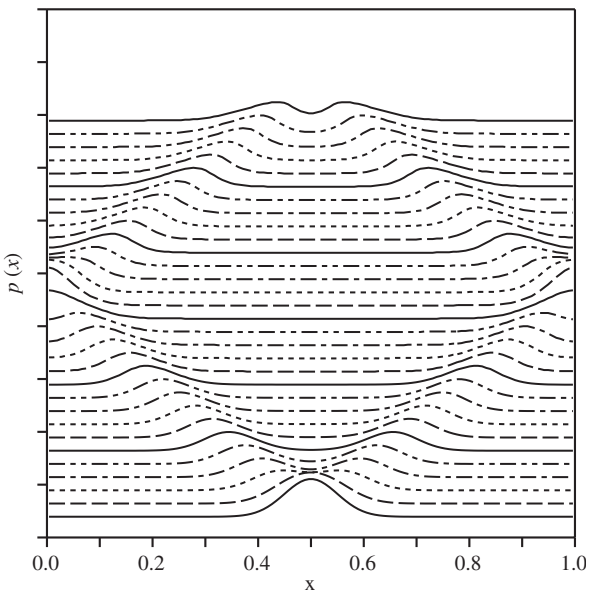

Figure 2. Linear wave evolution by original Euler equations.

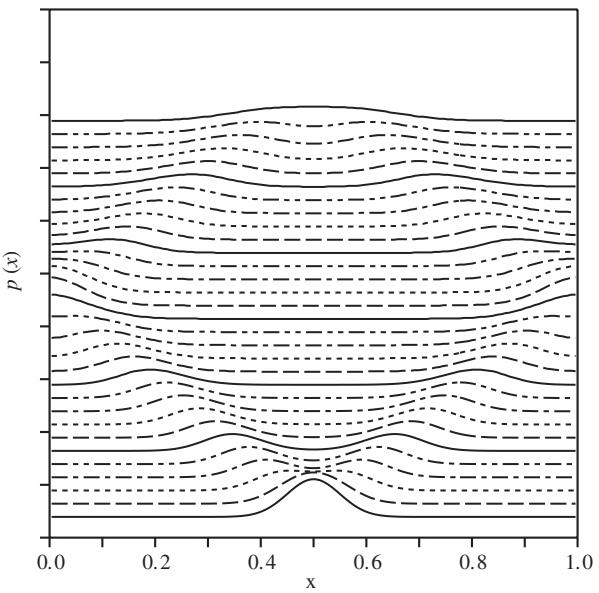

Figure 3. Linear wave evolution by modified Euler equations, with $l/\Delta x = 0.5$.

in both linear and non-linear case is the same and, in the above mentioned code, it's quite negligible ($\approx 1\%$). Larger values of l, although more effective in damping, require substantial decrease in the time-steps.

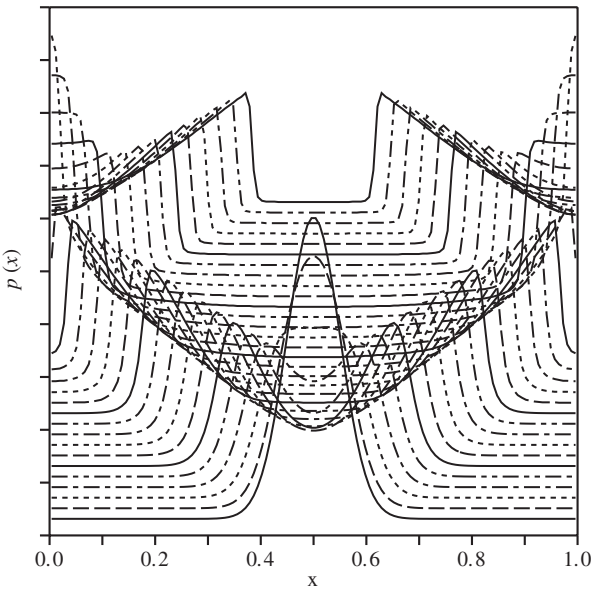

Figure 4. Non-linear wave evolution by the original Euler equations.

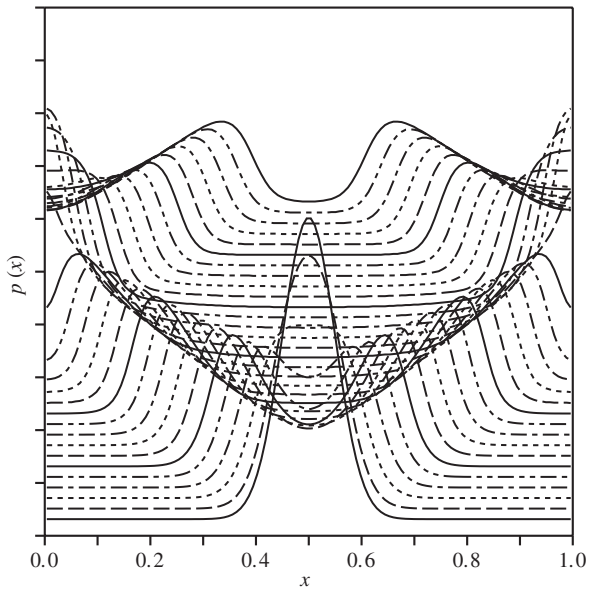

Figure 5. Non-linear wave evolution by the modified Euler equations. Here $l/\Delta x = 0.5$.

3.2. Implicit computations

To cure the stiffness generated by the new term, one needs to introduce some level of implicit evaluation to make high values of damping possible. Since the troublesome term appears only

in the momentum equation, only this equation needs to be treated implicitly. To do so, one finds it convenient to substitute for ρ_t in the momentum equation with $-(\rho u)_x$. The modified momentum equation is then:

$$(\rho u)_t + (p + \rho u^2)_x - l a_o (\rho u)_{xx} = 0$$

and its update formula is then:

$$(\rho u)_j^{n+1} = (\rho u)_j^n - \frac{\Delta t}{\Delta x}(F^{\star^n}_{2,j+1/2} + F^{\star^n}_{2,j-1/2}) - l a_o \frac{\Delta t}{\Delta x^2}((\rho u)_{j+1}^{n+1} - 2(\rho u)_j^{n+1} + (\rho u)_{j-1}^{n+1})$$

The last term (damping term) may not always vanish identically in the steady state. However, some loss of this desirable property seems to be inescapable with any conveniently implemented implicit scheme. In each time step, first $(\rho)^n$ and $(\rho E)^n$ is explicitly updated as usual, and then the discretized momentum equation is solved. The momentum equation results in an $N \times N$ tridiagonal system, where the diagonal terms are $(1 + 2\beta)$, the off-diagonal terms are $-\beta$, and

$$\beta = \frac{l a_o \Delta t}{\Delta x^2} > 0$$

Boundary conditions for the new term requires a value of ρu at ghost cells, which are trivial for the solid wall boundary. For other boundary conditions one may use the fact that $(\rho u)_{xx} = -(\rho_t)_x$ and

$$\rho_t = \frac{\rho_j^{n+1} - \rho_j^n}{\Delta t}$$

which gives the alternative form

$$(\rho u)_{xx}|_j^{n+1} = -\frac{(\rho_t)_{j+1} + (\rho_t)_{j-1}}{2\Delta x}$$

The unknowns are $(\rho u)_j^{n+1}$, and the right-hand side vector of the system is

$$\begin{pmatrix} \cdots + \beta(\rho u)_o^n \\ \cdots \\ (\rho u)_j^n - \frac{\Delta t}{\Delta x}(F^{\star^n}_{2,j+1/2} + F^{\star^n}_{2,j-1/2}) \\ \cdots \\ \cdots + \beta(\rho u)_{N+1}^n \end{pmatrix}$$

Note that the system is diagonally dominant, and can be efficiently solved by standard tri-diagonal solvers. The amount of extra work for solving this system is hardly visible.

Similar experiments to Section 3.1 are done to see by how much it is worth increasing this damping term. Figure 6 shows the linear wave (i.e. wave with small initial amplitude), with bulk viscosity corresponding to $l/\Delta x = 25$. For this data, the analysis of Section 2 predicts that any value of l greater than about $6\Delta x$ will result in very little wave propagation, and mostly static dissipation will happen. This is the effect seen in Figure 6. For high amplitude

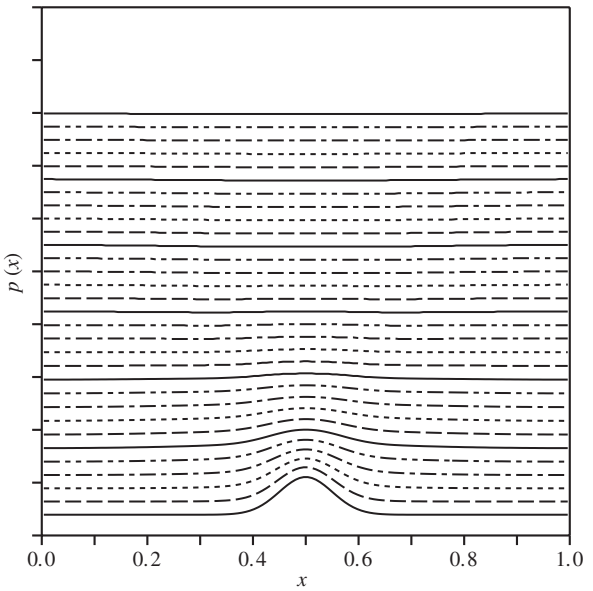

Figure 6. Linear wave evolution by modified Euler equations, $\frac{l}{\Delta x} = 25$.

waves, this linear analysis is not reliable. Experimentally, it seems that there is indeed little propagation, and that damping is rather slow. There is some disadvantage in not allowing the waves to get to the outer boundary, where a non-reflecting boundary condition could have helped to expel them. Figures 7 and 8 illustrate this. Later, our two-dimensional experiments will confirm that l should not in fact be taken too large.

4. GENERALIZATION TO TWO SPACE DIMENSIONS

4.1. Explicit computations

The modified momentum equations are:

$$\begin{aligned}(\rho u)_t + (p + \rho u^2)_x + (\rho uv)_y &= -l a_o \rho_{xt} \\ (\rho v)_t + (\rho uv)_x + (p + \rho v^2)_y &= -l a_o \rho_{yt}\end{aligned} \tag{10}$$

The other equations retain their original form.

We integrate Equations (10) over one numerical cell, and apply Green's theorem to get

$$\begin{aligned}(\rho u)_{ij}^{n+1} &= (\rho u)_{ij}^n - \frac{\Delta t}{\mathscr{A}} \sum F_{2n}^{\star} \Delta S - \frac{\Delta t.l.a_o}{\mathscr{A}} \oint_{\text{cell faces}} (\rho_t)\, \mathrm{d}y \\ (\rho v)_{ij}^{n+1} &= (\rho v)_{ij}^n - \frac{\Delta t}{\mathscr{A}} \sum F_{3n}^{\star} \Delta S + \frac{\Delta t.l.a_o}{\mathscr{A}} \oint_{\text{cell faces}} (\rho_t)\, \mathrm{d}x\end{aligned} \tag{11}$$

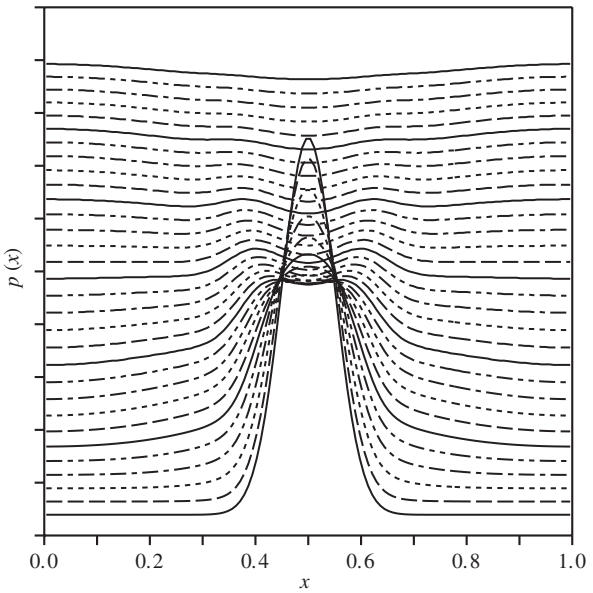

Figure 7. Non-linear wave evolution by modified Euler equations, $\frac{l}{\Delta x} = 25$.

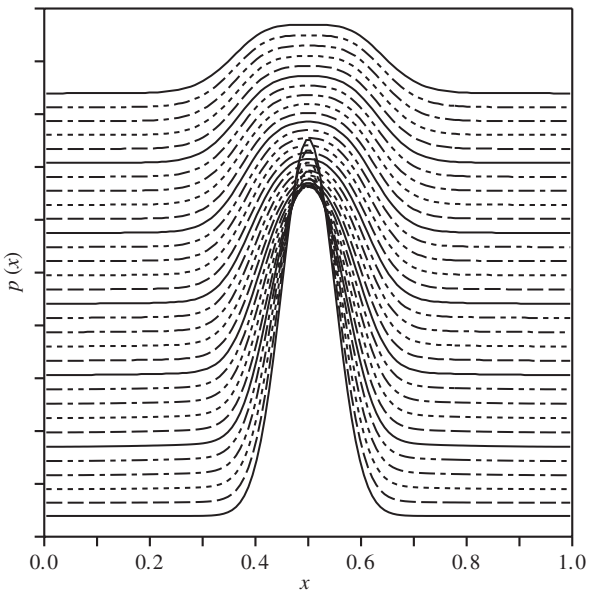

Figure 8. Non-linear wave evolution by modified Euler equations, $\frac{l}{\Delta x} = 100$.

Here $F_{2n}^{\star}$ and $F_{3n}^{\star}$ are second and third entries of the normal flux vector, computed using upwind or central differencing schemes.

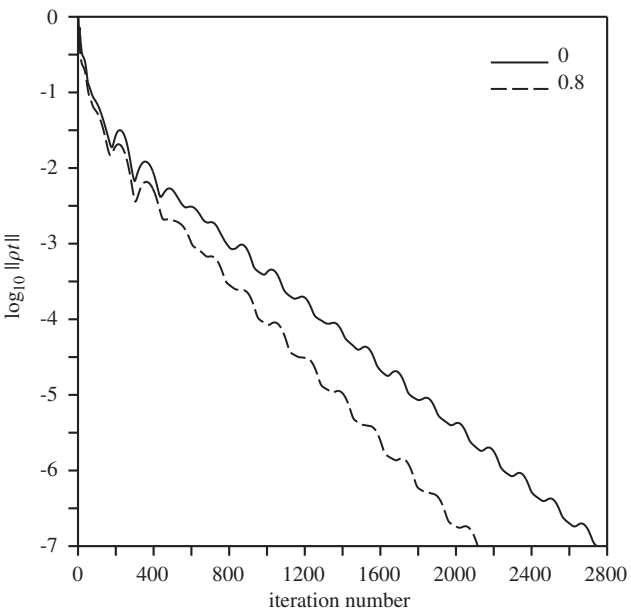

Figure 9. History of evolution of the residual $\frac{1}{N}\sum \log_{10} \|\rho_t\|$ for different values of $\frac{l}{\Delta x}$, showing the effect of adding bulk viscosity to a 1st-order upwind code.

One inexpensive way to evaluate ρ_t on the cell faces (for the line integral) is to take the average of the adjacent cells, to get:

$$\oint_{\text{cell faces}} (\rho_t)\,\mathrm{d}y = (\rho_t)_{i+1,j}\Delta y_{i+1/2,j} + (\rho_t)_{i,j+1}\Delta y_{i,j+1/2} + (\rho_t)_{i-1,j}\Delta y_{i-1/2,j} + (\rho_t)_{i,j-1}\Delta y_{i,j-1/2} \tag{12}$$

and a similar equation is found for y-momentum equation. To ensure stability, analogy with the one-dimensional case suggests that for explicit calculation, the value of l should be proportional to a local length scale, say, the average side length of the cell concerned.

Let us use the standard NACA0012 airfoil problem, for $M = 0.63$ and two degrees angle of attack. As a stable platform to test our modifications, first we use a first order upwind scheme. The surface boundary condition is the usual solid wall condition. The outer boundary is applied using the far field vortex solution. For the boundary condition for the new term, residuals are assumed to be zero in the ghost cells.

In Figure 9 the residual history for the original (non-viscous) code (solid line), and the code involving artificial bulk viscosity (dotted line) are compared. The history of the lift coefficient, for the same two codes, shows that the addition of bulk viscosity weakens the strong traversing waves. We ran experiments with much larger values of l, for which smaller timesteps were needed. This was to see whether an implicit code would be worth developing. The convergence history was plotted against a 'pseudo iteration number'

$$N^* = N \times \frac{\text{'inviscid' timestep}}{\text{actual timestep}}$$

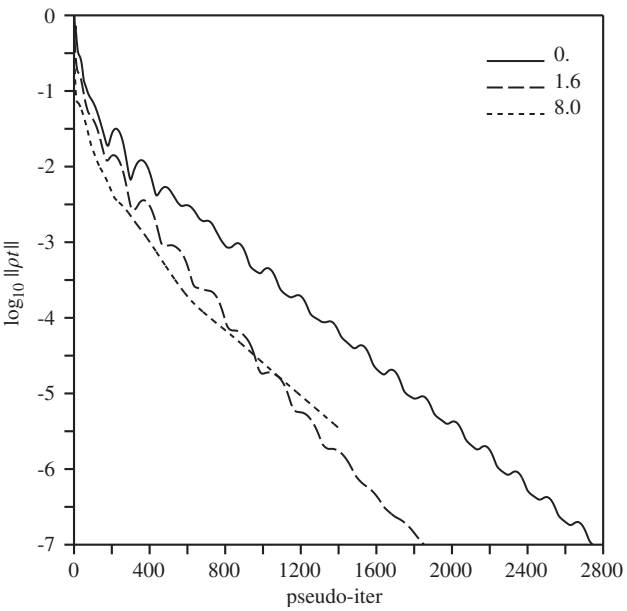

Figure 10. History of evolution of the residual $\frac{1}{N}\sum \log_{10} \|\rho_t\|$.

If the convergence had continued to improve on this basis, there would have been hope that an implicit code would have produced a similar history. In fact, Figure 10 shows that increasing the bulk viscosity is not always helpful. As in one space dimension, it seems that large values of bulk viscosity slow down the movement of the waves through the flow field, so that the basic mechanism of wave removal across the outer boundary is lost. In fact, there is always an optimum value of damping which maximize the convergence rate, and this value is usually upper but fairly close to the value of explicit implementation. Video movies showing the spatial distribution of the residuals show that using large values of l does damp out the waves during the early stages, but that a static pattern then develops that is very slow to disappear.

4.2. Implicit computations

To make higher values of bulk viscosity coefficients possible, implicit formulation of the momentum equations is necessary. The bulk viscosity components can be written in terms of ρu_{ij}^{n+1} and ρv_{ij}^{n+1} in many different ways, two of which are considered here [2].

In the first method, the average value of ρ_t in each face is found using continuity equation and Green's integral theorem on a suitable control volume in a three by three stencil around each cell. Finally this produces a system of linear equations very similar to a block-pentadiagonal system, which cannot be solved directly in $\mathcal{O}(n)$ time. The alternative is to use iterative methods, or ADI, the latter has been used here. Figure 11 shows the results of this method. Here the time-steps are determined only by CFL condition, and the code is stable for all values of l, but its time complexity constant (i.e. cpu time per iteration) is about 25% higher than the original code. One major problem here is that the BVD terms in the momentum equations (although very small) may not vanish in steady state.

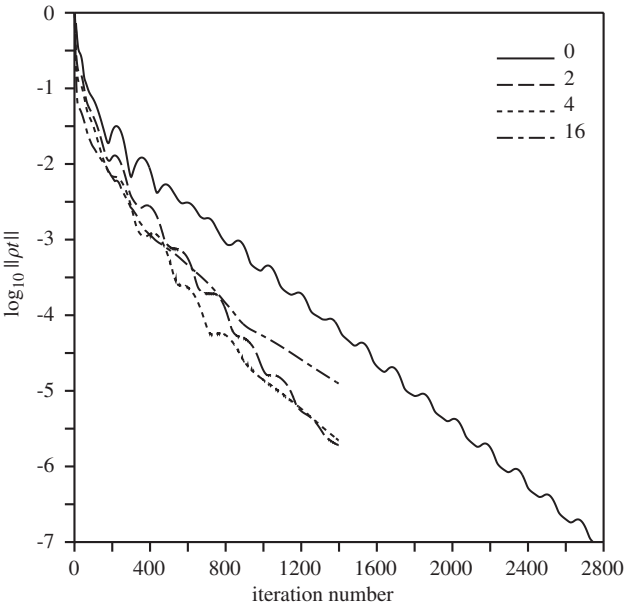

Figure 11. Residuals histories for different BVD coefficients resulting from the first implicit method.

In the second method, the following observation is made:

$$(\rho_{xt})^{n+1} = (\rho_{xt})^n + \Delta t(\rho_{xt})_t + \mathcal{O}(\Delta t^2) = (\rho_{xt})^n - \Delta t\{(\rho u)_x + (\rho v)_y\}_{xt} + \cdots$$
$$= (\rho_{xt})^n - \Delta t[((\rho u)_t)_{xx} + ((\rho v)_t)_{xy}] + \cdots$$

Then, Equations (10) can be rewritten correspondingly. Linearization of these equations and considering simple wave solution of them, shows that the new system is just a regular perturbation of the previous system, and for small time steps, it should resolve similar features as the original formulation of the bulk viscosity [2]. A method is introduced to implicitly discretize these equations. It finally reduces to a system of linear equations somehow similar to the first method, and finally produces fairly similar results (as Figure 11). The main advantage of this second method is that at steady state all the newly introduced terms vanishes (also confirmed experimentally).However, this time one cannot increase the BVD coefficient that much, and therefore the overall increase in convergence rate is not significant.

5. COMPARISON TO AND COMBINATION WITH OTHER TECHNIQUES

5.1. Residual smoothing

The maximum permissible time step for explicit calculation of Euler equations (before addition of BVD terms) is restricted by the stability limit on the Courant number. It was observed by Jameson [9] that this restriction can be relaxed by replacing the residual at each point by a weighted average of the neighbouring residuals. Consider a system of equations in one space

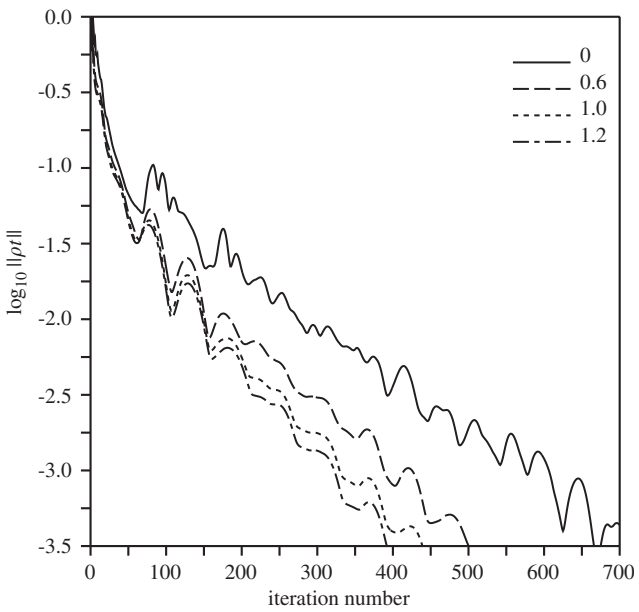

Figure 12. Comparison of residual history for different values of BVD in a central-differencing code.

dimension:

$$\mathbf{u}_t + \mathbf{f}_x = 0 \quad \mathbf{R}(\mathbf{u}) = -\mathbf{f}_x$$

where $\mathbf{u}, \mathbf{f} \in \mathbb{R}^n$, and $\mathbf{R}(\mathbf{u})$ is the vector of residuals. Residual smoothing consists of replacing $\mathbf{R}$ by a smoothed value $\bar{\mathbf{R}}$, defined either explicitly by:

$$\bar{\mathbf{R}} = (1 + \varepsilon_x \delta_x^2)\mathbf{R}$$

or implicitly by

$$(1 - \varepsilon_x \delta_x^2)\bar{\mathbf{R}} = \mathbf{R} \tag{13}$$

where δ_x is the central difference operator in the x-direction, and ε_x is the corresponding smoothing parameter. In two space dimensions, one may just add another term $(\varepsilon_y \delta_y^2)$ inside the parentheses. The best convergence rate of course depends upon the choice for the smoothing parameter. In practice the best convergence rate may be found by using Equation (13) and time-steps about three times larger than the Courant number of non-smoothed scheme, taking the smoothing parameter as large as possible while maintaining stability [9].

Performing this smoothing at the differential equation level for the one-dimensional acoustic equations gives

$$\rho_t + \rho_o u_x = \varepsilon \rho_{txx} \tag{14}$$

$$u_t + \frac{1}{\rho_o} p_x = \varepsilon u_{txx} \tag{15}$$

$$p_t + \rho_o a_o^2 u_x = \varepsilon p_{txx} \tag{16}$$

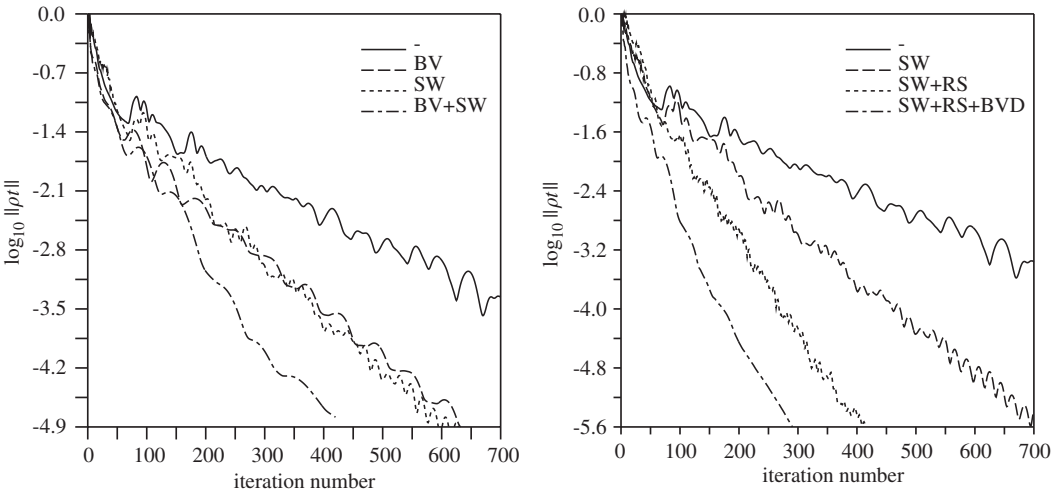

Figure 13. Combinations of the SWBC (with $\tau = 100\Delta t$, $\mu = 0.5$), BVD (with $l = 1.3\Delta S$), and RS (with $v = 2$, $\varepsilon = 0.2$) in the central-differencing code, at $M = 0.63$.

This changes the dispersion relationship to give

$$\frac{\omega_r}{\xi a_o} = \frac{\pm 1}{\sqrt{1 + \varepsilon\xi^2}} \tag{17}$$

with $\omega_i = 0$. This shows that residual smoothing works by decreasing the propagation speed, and does not, at the differential equation level, introduce damping at all. It can also be seen that it is chiefly effective at high frequencies. Since BVD does introduce damping, even at relatively low frequencies, it is expected that the two techniques will be complementary.

Experience shows that implicit implementation of RS is more effective. To implement RS in two space dimensions, using *approximate factorization* we write the 2D modified form of Equation (13) as

$$(1 - \varepsilon\delta_x^2)(1 - \varepsilon\delta_y^2)\bar{R}_{ij} = R_{ij}$$

and then we solve consecutively two tri-diagonal systems, generated from equations

$$(1 - \varepsilon\delta_x^2)Q_{ij} = R_{ij}^{n+1} \quad \text{and} \quad (1 - \varepsilon\delta_y^2)\bar{R}_{ij}^{n+1} = Q_{ij}$$

with appropriate boundary conditions. Applications of RS for solution of the previous external flow around NACA0012 airfoil, using a fairly coarse structured mesh with values of $v = 2.0$ and $\varepsilon = 0.2$, produces about 35% savings in total CPU time, and the residual history is very close to either dashed line in Figure 13(left).

5.2. *Soft wall boundary conditions (SWBC)*

In Reference [10] the idea was proposed of replacing the standard solid wall boundary conditions by something that allows incoming waves to be reflected with reduced amplitudes, over

an extended time. Such a condition can be written as

$$u_t + \frac{u}{\tau} = \frac{\mu}{\rho a} p_t$$

where τ, μ are parameters to be chosen from within certain not very critical ranges. In this work, we have used $\mu = 0.5$ and $\tau = 50\Delta t$ for solution of inviscid flow around a NACA0012 airfoil, at Mach 0.63, using a fairly coarse structured mesh. The numerical implementation is explained in Reference [2], and gains of up to 40% are found for subcritical flows (compare dashed and solid lines in Figure 13).

5.3. Combination of schemes in a central-differencing code

First we study the effect of adding BVD alone to a well established central differencing code. For the details of the central differencing code used here see References [11, 3]. We use the same standard NACA0012 airfoil problem as previously. Figure 12 compares the residual history for different values of bulk viscosity coefficient, added explicitly. It was found experimentally that the code is stable for values of l up to 1.3. The speedup due to BVD appears to be rather greater in this case than in our previous experiments with the upwind code. Presumably this is because we are dealing here with a second-order code, the regular form of which has less natural dissipation. The lift coefficient also converges very smoothly and very quickly to the correct steady state solution.

Figure 13 (left), shows the effect of combining BVD with the soft-wall BC. As compared with the basic method, if we require a four order of magnitude decrease in the value of the L_1 norm of residual, either modification by itself cuts the iterations to about 60% of the number originally required. In combination, the gains are multiplied, and only about 35% of the original iterations are needed. Combination of soft wall BC and RS is shown in Figure 13 (right, small dashed line), which is very similar to combination of soft wall BC and BVD (Figure 13 (left, dotted line)) and combination of BVD and RS (not shown here). We repeat that each modification adds negligible overhead to the time per iteration.

Finally Figure 13 (right, dotted line) shows the effect of combining all three acceleration methods. Now, only about 20% of the original iterations are required, and the overhead remains less than 5%. This plot confirms that bulk viscosity acts quite independently from other convergence acceleration schemes, with little overhead in CPU time per iteration.

6. LOW AND HIGH MACH NUMBERS

Central-differencing codes have generally been found to converge rather slowly for low Mach numbers. We discovered that adding a little BVD in explicit form not only makes the process very smooth and well-behaved, but also increases the convergence rate very significantly. To see the effect of BVD in low Mach number performance of central differencing codes, the same NACA0012 airfoil problem is used. In a Mach 0.3 case, CD codes with residual smoothing have difficulty in converging. Figure 14(a) shows the residual history for this airfoil problem. The number of iterations in this case is reduced by about 80% by BVD alone. It is interesting that the convergence plot is also far less 'noisy'. Figure 14(b) shows the time evolution of the lift coefficient for this computation. Here the oscillatory curve (solid line) corresponds

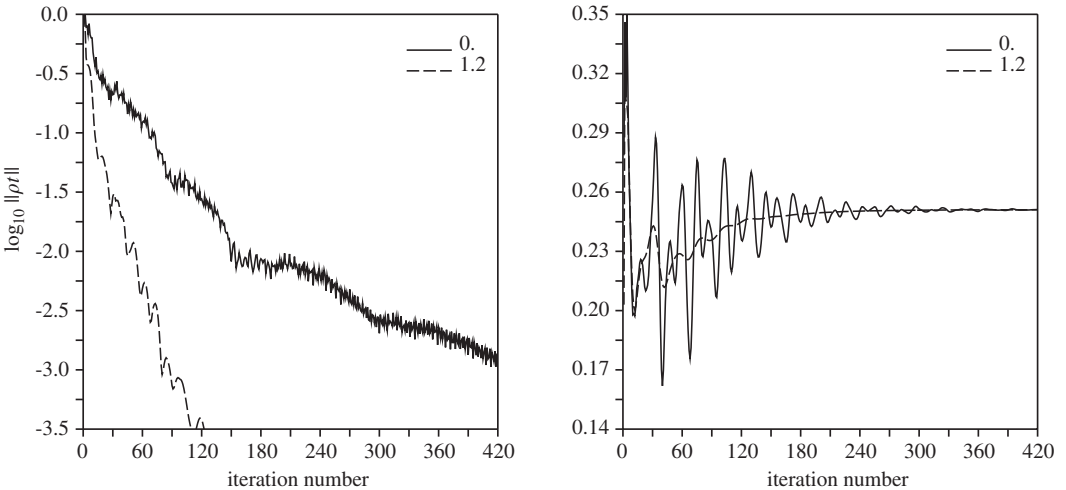

Figure 14. Effect of BVD combined with RS ($v = 2$ and $\varepsilon = 0.275$) in low Mach number flow $M = 0.3$, (a) residual history and (b) lift coefficient history.

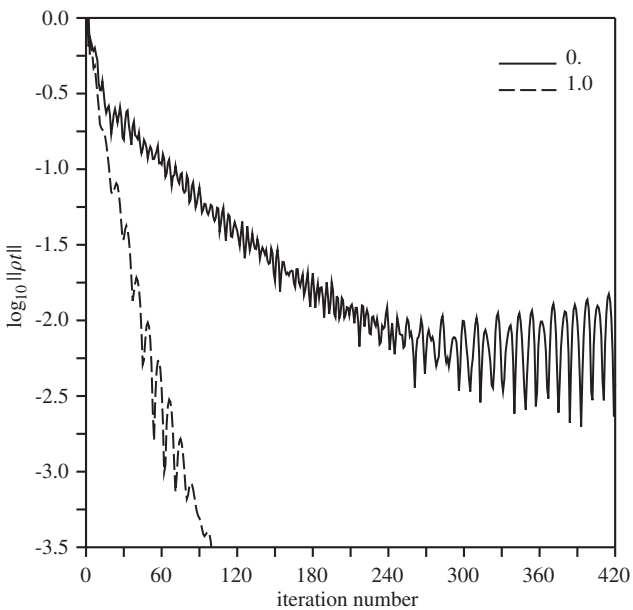

Figure 15. Effect of BVD combined with RS on the residual history for $M = 0.01$.

to the computation without BVD, and the smooth curve (dashed line) corresponds to adding BVD with bulk viscosity damping coefficient of $l = 1.2\Delta S$.

In the most extreme case, for Mach number $M = 0.01$, the regular code was unable to produce a converged solution, as shown in Figure 15. The solid line shows application of the

CD code with residual smoothing $\varepsilon = 0.2$ and the Courant number $\nu = 2.0$. The residual was reduced by about two orders of magnitude after 250 iterations, but then started to diverge. After explicitly adding a little BVD ($l = 1.0\Delta S$), the convergence is accelerated significantly in its first stages of computation, and the whole code is stabilized even for low values of residuals, and smooth convergence is achieved. A similar trend could be seen in the lift coefficient evolution curve.

Unfortunately, the bulk viscosity method turns out to be rather ineffective in transonic flow. In the best case the improvement is only just detectable, and in the worst case convergence is stalled. We believe that this can be explained in terms of the insights into convergence gained from the experiments reported in Reference [1]. The mechanism of convergence seems to be greatly altered by the presence of embedded shocks. On the one hand, these often absorb the wandering acoustic waves themselves, leaving little for BVD to accomplish. However, the shocks may be very slow to find their own final equilibrium positions, and this is usually the determining factor as regards transonic convergence. It seems to us that quite a different acceleration device is required in this case.

7. CONCLUSIONS

Bulk viscosity damping has been introduced, analysed, and applied to the Euler equations in one and two space dimensions. It was shown that BVD can be added as a simple module to most current codes written for subsonic compressible flows, and with no significant extra computation the rate of convergence can be increased significantly. The best value for the characteristic length required seems to be close to the local mesh size. With this choice, the time step of the regular inviscid code can be retained, or even increased if residual smoothing is employed. Larger values require elaborate implicit methods that do not pay off. With a simple explicit scheme, we have found gains of between 40 and 80%; the gains are most pronounced at low Mach numbers. The method complements very well other techniques for convergence acceleration. We have found that combining it with residual smoothing and a soft wall boundary condition is particularly effective, and carries an extremely low overhead.

ACKNOWLEDGEMENTS

The first author is sincerely grateful to the Aerospace Engineering Department of the University of Michigan for their generous support of this research.

REFERENCES

1. Mazaheri K, Roe PL. Numerical wave propagation and steady state solutions: Soft wall and outer boundary conditions. *AIAA Journal* 1997; **35**(6).
2. Mazaheri K. Numerical Wave Propagation and Steady State Solutions. *PhD Thesis*, University of Michigan, 1992.
3. Jameson A. Numerical Solution of the Euler Equations for Compressible Inviscid Fluids. In *Numerical Methods for the Euler Equations of Fluid Dynamics*, vol. 1, Angrand F, Dervieux A, Desideri JA, Glowinski R (eds). SIAM: Philadelphia, PA, 1985.
4. Strauss D, Azevedo JLF. Unstructured multigrid simulations of axisymmetric inviscid launch vehicle flows. In *19th AIAA Applied Aerospace Conference, AIAA Paper 2001-2476*, June, 2001.

5. McMullen M, Jameson A, Alonso JJ. Acceleration of convergence to a periodic steady state in turbomachinery flows. In *39th AIAA Aerospace Science Meeting, AIAA Paper 2001-0152*, January, 2001.
6. Puoti V. A preconditioning method for low speed flows. In *15th AIAA CFD Conference, AIAA Paper 2001-2555*, June, 2001.
7. Ramshaw JD, Mousseau VA. Accelerated artificial compressibility method for steady-state incompressible flow calculations. *Computers and Fluids* 1990; **18**:361–367.
8. Chorin AJ. A numerical method for solving incompressible viscous flow problems. *Journal of Computational Physics* 1967; **2**:12–26.
9. Jameson A. A vertex based multigrid algorithm for three dimensional compressible flow calculations. In *ASME Symposium on Numerical Methods for Compressible Flow*, Anaheim, 1986.
10. Mazaheri K, Roe PL. New lights on numerical boundary conditions. In *AIAA 10th Computational Fluid Dynamics Conference*, 1991.
11. Jameson A, Schmidt W. Turkel E. Numerical solutions of the Euler equations by a finite-volume method using Runge–Kutta time-stepping schemes. *AIAA Paper 81-1259*, 1981.

